JOURNAL OF CATALYSIS 32, 254–260 (1974)

The EPR Study of CO Adsorbed Ruthenium–Silica Catalysts

M. KOBAYASHI AND T. SHIRASAKI

Tokyo Institute of Technology, Research Laboratory of Resources Utilization, O-okayama, Meguro-ku, Tokyo 152, Japan

Received August 1, 1973

The adsorption of CO at 25–150°C on supported Ru-silica and Ru-graphite catalysts was studied by a pulse-flow system. For the CO-adsorbed Ru-silica catalyst, the EPR spectra were observed. The irreversible adsorption of CO showed its maxima at 60–100°C, and the $(CO/Ru)_c$ ratio (g-mole/g-atom), i.e., the ratio of the total amount of adsorbed CO per unit weight of catalyst (g-mole/g-catalyst) to the total amount of supported Ru-metal per unit weight of catalyst (g-atom/g-catalyst), for Ru-silica catalysts was more than unity; therefore, the existence of $Ru(CO)_3$, etc. were predicted. On the other hand, there were signals in the EPR spectra at a high adsorption temperature which corresponded to anisotropy in the g tensor. From the perturbation of ^2E–$^2A_1$ (C_{3v}) and e–b_2 (C_{4v}) in a strong-crystal-field model, the g-values were evaluated; the simulation curve agreed satisfactorily with that observed.

INTRODUCTION

In the preceding paper (*1*), we reported that the silica-supported ruthenium adsorbed a large quantity of CO at 150°C and that the volume of adsorbed CO per Ru-metal could not be used for the calculation of the metal surface area, and predicted the presence of $Ru(CO)_3$ and $Ru(CO)_4$ on the metal surfaces.

For comparison with McKee's report (*2*), the adsorption was carried out only at 150°C in the preceding paper (*1*); now we have attempted experiments for another temperature range in order to make sure that the supported Ru-metals adsorb CO abundantly, even at a temperature lower than 150°C; we have confirmed that, in the lower range of temperature, the $(CO/Ru)_c$ ratios (g-mole/g-atom), i.e., the ratio of the total amount of adsorbed CO per unit weight of catalyst (g-mole/g-catalyst) to the total amount of supported Ru-metal per unit weight of catalyst (g-atom/g-catalyst) were more than unity. Consequently, if a CO-molecule adsorbed on a Ru-atom in this experiment, the supported Ru-metal would be dispersed in the state of atoms or in the state of crystal unit cells and all Ru-atoms would combine with CO-molecules. Virtually, the supported Ru-metal exists in the state of metal particles which diameter are more than 10 Å and significant amounts of these Ru-atoms exist inside of the particles, so that CO-molecules which are at least more than 1, adsorb on a Ru-atom which is exposed on the surface of these particles.

Moreover the EPR spectra of these CO-adsorbed samples were observed, and three main signals which were attributable to anisotropy in the g tensor, were obtained. The g-values of these spectra coincided with those evaluated from Ru^{3+} and Ru^{4+} by means of the crystal field theory.

EXPERIMENTAL METHODS

The experimental method for CO adsorption was the pulse-flow system described in the preceding paper (*1*). Three sorts of Ru-catalysts supported on silica gels and graphite were used. Ru–SiO_2-35-1 and Ru–SiO_2-30-2 were the same catalysts which had already been used in a previous study (*1*). The Ru–G-3 catalyst, which was

supported on graphite, contained 0.0202 mg-atom Ru/g, and its specific surface area was 15 m^2/g. The activities of these catalysts for the dehydrogenation of cyclohexane have been reported (*3*, *4*).

The EPR spectra were observed by means of a "Varian E-12-type" spectrometer (X band, modulation frequency 100 kHz). About 0.1 g portion of the samples (about 30 mesh) were placed at the bottom of a U-shaped tube similar to Hukuda and Amenomiya report (*5*). After the adsorption of CO at 100–150 mm Hg for 2–12 hr in the usual static system, and after evacuation at the same temperature as the adsorption for 2 hr, the samples were slipped down to the quartz tube for spectroscopic analysis. The quartz tube was then sealed, cut off, and used for the observation. Almost all of the spectra were observed at -170°C and at the microwave frequency of $\nu = 9.135$ GHz. Except for the sample which adsorbed CO at 25°C, the spectra which were observed at room temperature were not sharp. For the EPR spectra, only the Ru–SiO_2-30-2 catalyst was used, because its silica gel supporter did not contain paramagnetic impurities.

Results

The experimental data of CO adsorption are summarized in Table 1. Figure 1 illustrates the total amount of adsorbed CO (g-mole) per total amount of Ru-metal (g-atom) which was supported on silica gels [(○) Ru–SiO_2-35-1, (□) Ru–SiO_2-30-2] and graphite [(△) Ru-G-3] at various temperatures (25, 60, 100, 150°C). The irreversible values of $(CO/Ru)_c$ for Ru–SiO_2-35-1 (specific surface areas including supporter: $S_g = 242$ m^2/g) and Ru–SiO_2-30-2 ($S_g = 91$ m^2/g) are almost the same and more than unity except for the one at 25°C, and show their maxima at 60 and 100°C for each catalyst. For example, from the values of v_c at 60°C in Table 1 and $v_{CO}/S_g = 0.1$ (ml/m^2) which was determined for Ru-metal powder in the preceding paper (*1*), we can get the exposed Ru-metal surface area about 102, 28 and 2.2 (m^2/g-catalyst) for Ru–SiO_2-35-1, Ru–SiO_2-30-2 and Ru-G-3, respectively. These values are too large compared with S_g of their supporters. These results are therefore in conflict with the fact that S_g does not change by the small amount (less than 3 wt%) of metal supporting. Consequently, the value $v_{CO}/S_g = 0.1$ (ml/m^2) for metal powder can not be applicable to the supported metal.

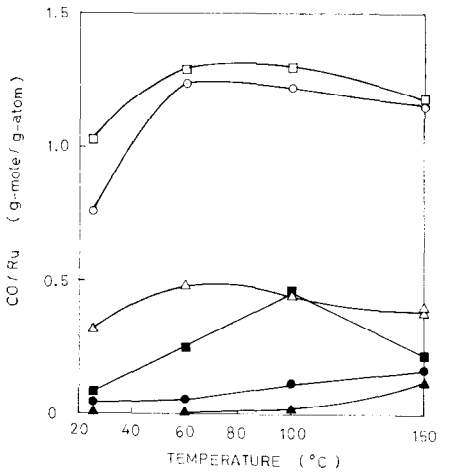

FIG. 1. Adsorption of CO on supported Ru-catalysts by pulse-flow system. (○) Ru–SiO_2-35-1, (□) Ru–SiO_2-30-2, (△) Ru-G-3; (open symbols) irreversible $(CO/Ru)_c$, (closed symbols) reversible $(CO/Ru)_p$.

The smaller irreversible value of $(CO/Ru)_c$ at 25°C may be attributed to the relation between the rate of adsorption and the dynamic state of the pulse-flow system. With this in mind, the sample of Ru–SiO_2-30-2 for the EPR spectra at 25°C was allowed to adsorb CO for over 12 hr in the static system. The reversible value of $(CO/Ru)_p$ tends to increase with the rise in the temperature. This phenomenon can be explained as resulting from the definition of the reversible adsorption in the pulse-flow system, as has been described in the preceding paper (*1*), that is, first, the sum of the irreversible and reversible adsorptions is measured; the readsorption after exposure to the He carrier for 2 hr is regarded as the reversible adsorption. Consequently, at high temperatures, volatile Ru-carbonyl compounds are formed and are carried away during the exposure, so the value of

TABLE 1
CO ADSORPTION ON THE SUPPORTED RUTHENIUM CATALYSTS AT VARIOUS TEMPERATURES[a]

Catalysts	Temp (°C)	25	60	100	150
Ru–SiO_2-35-1	v_c[ml(STP)/g]	6.26	10.20	10.04	9.42
	v_p	0.432	0.494	0.996	1.428
Ru–SiO_2-30-2	v_c	2.24	2.79	2.81	2.55
	v_p	0.186	0.552	0.998	0.476
Ru-G-3	v_c	0.1467	0.219	0.205	0.175
	$v_p \times 10^2$	0.814	0.723	0.845	5.63

[a] Subscripts: *c*, irreversible; *p*, reversible.

readsorption (i.e., the reversible adsorption) increases.

The EPR spectra of Ru–SiO_2-30-2, which adsorbed CO at various temperatures, are shown in Fig. 2. Each spectra has a signal corresponding to the *g*-value of 1.99, and with the rise in the adsorption temperature two main signals appear in the low magnetic field. These signals show the existence of anisotropy in the *g* tensor; the principal elements of the spectroscopic splitting factor will be evaluated in the next section. For the sample which adsorbed CO at 25°C, the spectra at both room temperature (about 20°C) and −170°C (Fig. 2b) were observed.

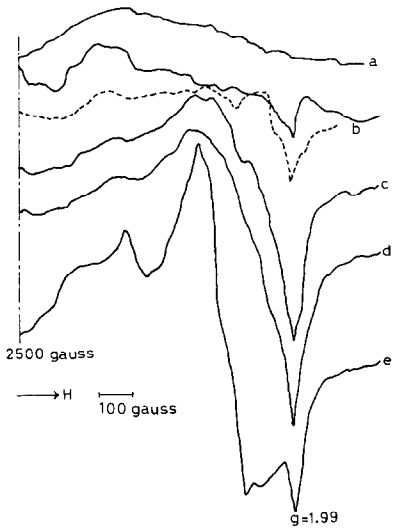

FIG. 2. EPR spectra of CO adsorbed Ru–SiO_2 catalyst. (a) Blank, CO adsorption temperature: (b) 25°C, (c) 60°C, (d) 100°C, (e) 150°C; spectra observation temperature: (—) −170°C, (- - -) room temperature (20°C).

DISCUSSION

From the results shown in Fig. 1 and in the preceding paper (*1*), it can be presumed that there are $Ru(CO)_2$, $Ru(CO)_3$, $Ru(CO)_4$, etc., in addition to Ru(CO) on the surface of Ru-metal.

With decreasing crystallite size of metal particles, the proportion of surface atoms of low coordination will increase. As well-known in metallurgy, dislocation, grain boundary and phase boundary are unstable, but atomic vacancies have a thermal equilibrium concentration in fine particles, and these vacancies correspond to step kinks on the surface of crystal particles. It will be reasonable that $Ru(CO)_2$, $Ru(CO)_3$ and $Ru(CO)_4$ may be formed on the low coordinate Ru-atoms of step kinks which will exist numerously in our highly dispersed catalysts.

There is a great difference of the EPR spectra (Fig. 2) between 100 and 150°C in the adsorption temperature, in spite of the almost same value of $(CO/Ru)_c$ (Fig. 1). The fact suggests that the changes of bond structures between a Ru-atom and C-atoms, e.g., $[Ru(CO)_2]^+(CO)^- \rightarrow Ru(CO)_3$ $[Ru(CO)]^{2+}(CO)_2^{2-} \rightarrow Ru(CO)_3$, etc., occur and that these changes need some activation energies. In the changes of bond structures, electrons will be donated or back-donated between a Ru-atom and carbon atoms by σ-orbitals or π-orbitals, and the migration of electrons will be easy at high temperature because of the occupation of antibonding orbitals.

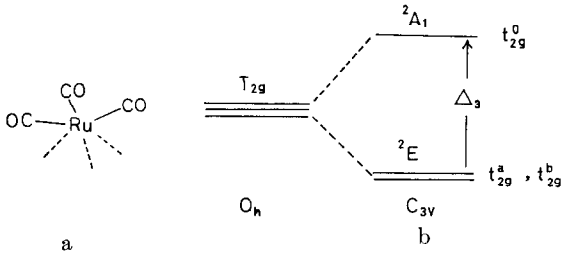

FIG. 3. A model of $Ru(CO)_3$ and the splitting of energy levels in C_{3v}

Exact analysis of these hyperfine structure or σ–π interaction, etc., by the molecular orbital theory may not be applicable to the EPR spectra which were obtained in the solid state and were not sharp, so we attempted the approximation by crystal field theory and the analysis of $[Ru(CO)_2]^+(CO)^-$, $[Ru(CO)]^{2+}(CO)_2^{2-}$, $[Ru(CO)]^{3+}(CO)_3^{3-}$, etc., was omitted. In the approximation, the bond structures between Ru-atoms (broken line in Figs. 3a and Fig. 4a) were neglected and the bonds between a Ru-atom and C-atoms were considered. At first the application of the g tensor without axial symmetry was done, but one component of the g tensors for Ru ion which has more than five electrons in the d-shell, became smaller than 2. This is not the case for the experimental results (Fig. 2) in which all g-values are equal to 1.99 or larger than 1.99 (1.99 corresponds to 2.00 without the orbital reduction factor k), so that axial symmetry was postulated.

In the case of Ru(CO), $Ru^+(4d^7)$ may be regarded as a three-hole state, t_{2g}^{3p}. From this electron configuration, it is difficult to determine the zero-order wavefunction. The $C_{\infty v}$ symmetry can be postulated, so that all the degeneracy will be resolved except for Kramer's degeneracy and only $g_\parallel = 2.00$ will be obtained with respect to the excited levels.

In the case of $Ru(CO)_2$, $Ru^{2+}(4d^6)$ is a closed-shell configuration (t_{2g}^6) in a strong-crystal-field model, so this complex must be diamagnetic (*6*). The existence of $Ru(CO)_2$ can not be confirmed by the EPR spectra because of the diamagnetism.

In the case of $Ru(CO)_3$, the C_{3v} symmetry was postulated for $Ru^{3+}(4d^5)$ as shown in Fig. 3a, so that this low-spin d^5 compound has two distinct g-values, $g_\parallel$ and $g_\perp$. As t_{2g}^6 is a closed-shell configuration, t_{2g}^{5e} may be regarded as a one-hole state, t_{2g}^p. It is assumed that a low-symmetry C_{3v} perturbation separates the one-hole real functions, t_{2g}^a, t_{2g}^b, and t_{2g}^0, which are quantized by a 3-fold axis. Their energy levels are split by the crystalline field, C_{3v}, as is described in Fig. 3b. These functions, t_{2g}^a, t_{2g}^b, and t_{2g}^0, are given in Eq. (1) as a linear combination of d-orbitals, which were derived by Ballhausen (*6*):

$$\begin{cases} t_{2g}^0 = d_0 \\ t_{2g}^a = (2/3)^{1/2}d_2 - (1/3)^{1/2}d_{-1} \\ t_{2g}^b = (2/3)^{1/2}d_{-2} + (1/3)^{1/2}d_1. \end{cases} \quad (1)$$

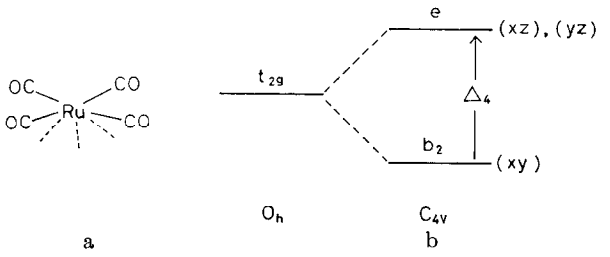

FIG. 4. A model of $Ru(CO)_4$ and the splitting of energy levels in C_{4v}.

For the degenerate ground state, ^2E (t_{2g}^a, t_{2g}^b), in Fig. 3b the principal values of the g tensor were estimated from the Hamiltonian in the Zeeman effect. From the results of

$$\langle t_{2g}^a\alpha|L_z + 2S_z|t_{2g}^a\alpha\rangle = 2,$$
$$\langle t_{2g}^b\alpha|L_x + 2S_x|t_{2g}^b\beta\rangle = 1, \text{etc.}, g_\parallel = g_\perp = 2$$

is derived, and the spin–orbit interaction in $t_{2g}^a\alpha$, $t_{2g}^b\beta$, etc., becomes 0, so the mixing of the ground state, ^2E, and the excited state, $^2A_1$, in the spin–orbit interaction should be considered in explaining the existence of anisotropy in the g tensor. The mixing is the same as the Kramer doublet derived by Stevens (*7*), as is shown in Eq. (2):

$$\begin{cases} \psi_{1/2} = at_{2g}^0\alpha + bt_{2g}^b\beta \\ \psi_{-1/2} = at_{2g}^0\beta - bt_{2g}^a\alpha. \end{cases} \tag{2}$$

The orbital reduction factor, k, was used when the eigenvalues of the spin–orbit Hamiltonian were estimated from the first-order perturbation. The results were:

$$\langle\psi_{1/2}|kL_z + 2S_z|\psi_{1/2}\rangle = a^2 - (k+1)b^2,$$
$$\langle\psi_{1/2}|kL_x + 2S_x|\psi_{-1/2}\rangle = a^2 + 2^{1/2}abk - b^2/3,$$

etc. The g-values are:

$$\begin{aligned} g_\parallel &= 2[a^2 - (k+1)b^2], \\ g_\perp &= 2[a^2 + 2^{1/2}kab]. \end{aligned} \tag{3}$$

The matrix of the perturbation is:

$$\begin{vmatrix} -2D_\sigma - 6D_\tau - E & \xi/\sqrt{2} \\ \xi/\sqrt{2} & D_\sigma + 2D_\tau/3 + \xi/2 - E \end{vmatrix}, \tag{4}$$

where D_σ and D_τ are the splitting parameters in a trigonal crystal field (*6*) and where ξ is the spin–orbit coupling constant. From the Hamiltonian, $\mathfrak{U}_\tau$, of a trigonal crystal field, the energy levels are:

$$\begin{aligned} \langle t_{2g}^0|\mathfrak{U}_\tau|t_{2g}^0\rangle &= -2D_\sigma - 6D_\tau, \\ \langle t_{2g}^b|\mathfrak{U}_\tau|t_{2g}^b\rangle &= D_\sigma + 3D_\tau/2. \end{aligned} \tag{5}$$

Therefore:

$$\Delta_3 = (D_\sigma + 3D_\tau/2) - (-2D_\sigma - 6D_\tau), \tag{6}$$
$$\Delta E = [(\Delta_3 + \xi/2)^2 + 2\xi^2]^{1/2}, \tag{7}$$
$$\Delta E/\xi = f, \tag{8}$$
$$x = \{[\xi^2(f^2 - 2)]^{1/2} - f\xi\}/2. \tag{9}$$

From Eqs. (4)–(9), Eq. (3) becomes as follows:

$$\begin{aligned} g_\parallel &= 2[\xi^2 - 2(k+1)x^2]/(2x^2 + \xi^2), \\ g_\perp &= 2(\xi^2 - 2kx\xi)/(2x^2 + \xi^2). \end{aligned} \tag{10}$$

We could not find the experimental values of the transition energy in the electronic spectra of ruthenium-carbonyles [$Ru(CO)_5$, $Ru_3(CO)_{12}$], which are most representative as substitutes for the CO adsorbed Ru, so we used Hudson and Kennedy's datum, $f = 8.22$ (*8*), which was calculated from the $RuCl_3(PMe_2Ph)_3$ complex in order to get the numerical values of $g_\parallel$ and $g_\perp$. The spin–orbit coupling constant, $\xi = -884$ cm^{-1}, which was reported in Hudson and Kennedy's study (*8*) was also used. The only reasonable g-values which were near to the experimental data were $g_\parallel = 1.96$, $g_\perp = 2.19$, and $k = 0.86$, which were calculated from all the combinations of k, ξ, and f by means of a Fortran computer program.

The ground state, ^2E, in Fig. 3b is degenerate, so the formulation given by Pryce (*9*):

$$g_{ij} = 2\left(\delta_{ij} - \xi\sum_{n\neq 0}(\phi_0|L_i|\phi_n)(\phi_n|L_j|\phi_0)/(E_n - E_0)\right), \tag{11}$$

should not be used immediately in order to estimate the g tensor from the second-order perturbation theory, but since, as a result, all the eigenvalues of the spin–orbit Hamiltonian,

$$\langle t_{2g}^a\alpha|\xi\mathbf{L}\cdot\mathbf{S}|t_{2g}^b\beta\rangle,$$

etc., become 0, Eq. (11) may be used. Then:

$$\begin{aligned} &\phi_0 = t_{2g}^a, \quad \phi_n = t_{2g}^0, \\ &g_{ij} = 2(\delta_{ij} - \xi\Lambda_{ij}), \\ &\Lambda_{xx} = \langle t_{2g}^a|L_x|t_{2g}^0\rangle\langle t_{2g}^0|L_x|t_{2g}^a\rangle/\Delta_3 = 1/2\Delta_3, \\ &\Lambda_{zz} = \langle t_{2g}^a|L_z|t_{2g}^0\rangle\langle t_{2g}^0|L_z|t_{2g}^a\rangle/\Delta_3 = 0, \\ &g_\parallel = g_{zz} = 2, \\ &g_\perp = g_{xx} = 2(1 - \xi/2\Delta_3). \end{aligned} \tag{12}$$

The numerical g-values were found to be $g_\parallel = 2$, and $g_\perp = 2.20$ by using Hudson and Kennedy's datum $f = 8.22$; these results are almost the same as those of the first-order perturbation.

In the case of $Ru(CO)_4$, a C_{4v} symmetry was postulated for $Ru^{4+}(4d^4)$ as shown in Fig. 4a. In the strong-crystal-field model, $(t_{2g})^4$ may be regarded as a two-hole state, i.e., $(t_{2g})^2$. The splitting of these energy levels is described in Fig. 4b. Here, the two electron configuration which corresponds to the two energy levels, e and b_2, must be examined in order to get the eigenfunctions. At first, in the case of the spin triplet, i.e., $S = 1$, $(e)(e)$ and $(b_2)(e)$ are possible for the two-electron configuration of C_{4v} on the bases of the Pauli principle. For the $(e)(e)$ configuration, θ is obtained for the orbital function as an irreducible representation, $^3A_2$; then:

$$\theta(^3A_2) = |(xz)(yz)|. \tag{13}$$

For the $(e)(b_2)$ configuration also,

$$\begin{aligned} \phi_1(E) &= |(xy)(yz)|, \\ \phi_2(E) &= |(xy)(xz)|. \end{aligned} \tag{14}$$

Here, the combination with the spin function ψ $(S = 1)$ may be considered; then:

$$\begin{aligned} \psi_1 &= \alpha\alpha, \\ \psi_0 &= (\alpha\beta + \beta\alpha)/\sqrt{2}, \\ \psi_{-1} &= \beta\beta. \end{aligned} \tag{15}$$

From the eigenfunctions $\phi_1\psi_1$, $\phi_1\psi_{-1}$, $\phi_2\psi_1$, $\phi_2\psi_{-1}$, etc., in the ground state, the g-values become 2, so that the mixing of $\theta(^3A_2)$ and $\phi(E)$ must be considered for the existence of $g > 2$. By the C_4 and C_2 operation in C_{4v}, it was found that the groups of θ_1, θ_3 $(^3A_2)$ and Ψ_1, Ψ_2 (E) belonged to the same irreducible representation of double groups, Γ_5, as follows:

$$^3A_2(\Gamma_5) \quad \begin{cases} \theta_1 = \theta\psi_1 \\ \theta_3 = \theta\psi_{-1}, \end{cases} \tag{16}$$

$$E(\Gamma_5) \quad \begin{cases} \Psi_1 = \phi_1\psi_0 \\ \Psi_2 = \phi_2\psi_0. \end{cases} \tag{17}$$

Further, it may be necessary to mix the linear combinations of Ψ_1 and Ψ_2, which are diagonal, with θ_1 and θ_3 in a 4-fold axis. From a transformation by the C_4 operation, the results become:

$$\begin{aligned} \Psi'_1 &= (i\phi_1\psi_0 + \phi_2\psi_0)/\sqrt{2}, \\ \Psi'_2 &= (i\phi_1\psi_0 - \phi_2\psi_0)/\sqrt{2}. \end{aligned} \tag{18}$$

The pair of Ψ'_1 and θ_1 and the pair of Ψ'_2 and θ_3 can be miscible with each other in spin–orbit interaction. Then:

$$\langle\Psi'_1|\lambda\mathbf{L}\cdot\mathbf{S}|\theta_1\rangle = \lambda/2, \tag{19}$$

where λ is a spin–orbit coupling constant in the multielectron state. Consequently, from the first-order perturbation the linear combination of ground and excited states is:

$$\begin{aligned} \Psi(\Gamma_5^1) &= \Psi'_1 - \lambda\theta_1/2\Delta_4, \\ \Psi(\Gamma_5^2) &= \Psi'_2 - \lambda\theta_3/2\Delta_4. \end{aligned} \tag{20}$$

The eigenvalues of the Hamiltonian in the Zeeman term become:

$$\begin{aligned} &\langle\Psi(\Gamma_5^2)|kL_z + 2S_z|\Psi(\Gamma_5^2)\rangle \\ &\qquad = k, \\ &\langle\Psi(\Gamma_5^1)|kL_x + 2S_x|\Psi(\Gamma_5^2)\rangle \\ &\qquad = -1 + \lambda(1 + k)/\Delta_4, \end{aligned}$$

etc.,

where the second power of the term of λ is neglected. Then, the g-values are:

$$\begin{aligned} g_\parallel &= 2k, \\ g_\perp &= 2 - \lambda(k + 1)/\Delta_4. \end{aligned} \tag{21}$$

In the calculation of the numerical g-values, we used Hudson and Kennedy's data (*8*):

$$E_e/\xi = -1.02,\ E_{b2}/\xi = 2.04,$$

and $\xi = -1180$ cm^{-1}, which are derived from Ru^{3+} in D_{4h}; then, $\Delta_4 = E_e - E_{b2} = 3610$ cm^{-1}.

Moreover, we adopted $\xi = -1350$ cm^{-1} for the Ru^{4+} free ion, as an approximate value, which has been reported by Figgs and Lewis (*10*); then:

$$\lambda = \xi/2S = -675 \text{ cm}^{-1} \text{ where } S = 1,$$

and $g_\parallel = 1.99$, $g_\perp = 2.37$, and $k = 0.99$.

In the case of the spin singlet $S = 0$ in C_{4v}, there is no eigenfunction which is miscible with the others, so the g-values are always 2 or 0.

Because of the complexity, we did not

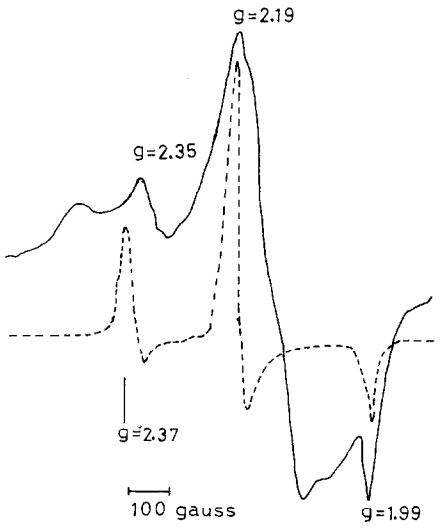

FIG. 5. Simulation curve in the anisotropy g-values. (—) Experimental, (– –) simulation.

attempt to calculate the second-order perturbation in C_{4v} or the interaction with the more excited levels which are split from $E_g(O_h)$. We also did not examine the zero-field splitting, because the g-values of all the experimental data are always equal to 1.99 or more than 1.99.

With the g-values which are obtained from $Ru(CO)_3$ and $Ru(CO)_4$, a simulation curve is calculated; it is shown in Fig. 5, in which the spectra of $Ru(CO)_3$ and $Ru(CO)_4$ overlap. The observed spectrum in Fig. 5 is modified by removing the background in Fig. 2a, from the original spectrum in Fig. 2e. Although some parts of the simulated spectrum differ from the observed one, the agreement is considered satisfactory with regard to the three main peaks. The difference between the experimental value, $g = 2.35$, and the calculated one, $g = 2.37$, arises from the approximation in which the ξ of the free ion was used in the calculation of the energy, Δ_4. In conclusion, it seems certain that there are $Ru(CO)_3$ and $Ru(CO)_4$ in the Ru-silica catalyst which adsorbed CO at high temperatures. We could not detect the existence of Ru^{2+} because of its diamagnetism, but the formation of $Ru(CO)_2$ may be presumed.

ACKNOWLEDGMENTS

The authors thank Mr. Y. Nakamura (Tokyo Institute of Technology, Research Laboratory of Resources Utilization) for his measurement of the EPR spectra.

REFERENCES

1. KOBAYASHI, M., AND SHIRASAKI, T., *J. Catal.* **28**, 289 (1973).
2. MCKEE, D. W., *J. Catal.* **8**, 240 (1967).
3. KOBAYASHI, M., FUKUDA, S., AND SHIRASAKI, T., *Nippon Kagaku Kaishi* 464 (3) (1973).
4. KOBAYASHI, M., AND SHIRASAKI, T., *Kagaku kogaku* **37**, 165 (1973).
5. HUKUDA, K., AND AMENOMIYA, Y., *Can. J. Chem.* **49**, 352 (1971).
6. BALLHAUSEN, C. J. "Introduction to Ligand Field Theory." McGraw-Hill, New York, 1962.
7. STEVENS, K. W. H., *Proc. Roy. Soc. Ser. A* **219**, 542 (1953).
8. HUDSON, H., AND KENNEDY, M. J., *J. Chem. Soc. A* **1969**, 1116.
9. PRYCE, M. H. L., *Proc. Phys. Soc., London, Sect. A* **63**, 25 (1950).
10. FIGGS, B. N., AND LEWIS, J., *Progr. Inorg. Chem.* **6**, 37 (1964).